JMEPEG (2004) 13:548-556
DOI: 10.1361/10599490420575

1059-9495/$19.00

Numerical Analysis of Shear Deformation Localization Using a Double-Variable Damage Model

T.C. Lee, C.Y. Tang, and L.C. Chan

(Submitted January 20, 2004)

A double-variable damage model was introduced into the constitutive equations to demonstrate the effect of the material damage for the isotropic elastic, hardening, and damage states, and for the isothermal process. The shear damage variable D_s and the bulk damage variable D_b may be, respectively, used to describe the effect of shear damage and bulk damage for material properties without the superfluous constraint, $D_b = D_s$, that is found in the single-variable damage model. The double-variable damage model was implemented to form the finite element code for analyzing the effect of shear damage and bulk damage. In this article, two numerical simulation examples were completed to model the whole process of initiation and propagation of shear bands in an aluminum alloy. The numerical computational results are coincident with the experimental results.

Keywords double-variable damage model, isotropic damage, numerical modeling, shear damage, shear deformation localization

1. Introduction

In some metal-forming processes, such as fine blanking and side pressing, shear deformation localization may occur. It is often found through microscopic observation that there are some microstructure changes, such as microcracking, grain boundary debonding, particle cracking, and microshear banding, in the shear deformation localization area.[1,2] Microscopic damage often leads to a material softening and a reduction in material properties. This can increase the plastic deformation in the area, leading to deformation localization. Therefore, it is feasible to study shear deformation localization from a damage viewpoint.

The fundamentals of the analysis of deformation localization in elastic-plastic solids have been developed by Hill[3] and Rice.[4] Some researchers have studied deformation localization from a plastic instability viewpoint.[5] Others have subsequently studied the problem to determine the forming limit diagram using a damage mechanics method.[6,7] Saanouni et al.[8] introduced damage variables into constructive equations to model the initiation and propagation of deformation localization. The direct damage mechanics approach can account for material degeneration induced by material damage in the deformation localization process compared with the limit diagram in the damage approach. So, this approach can better model deformation localization processes, such as necking and shear banding.

Continuum damage mechanics (CDM) has been greatly developed since Kachanov proposed the initial model in 1958, in that the loss of stiffness can be measured by a macroscopic damage parameter. Lamaitre[9] systematically proposed a set of constitutive equations, including a damage variable and the corresponding damage evolution equation, on the basis of thermodynamics. His work made a remarkable contribution in establishing the tenets of phenomenological damage theory. Chow and Wang[10-12] made important progress in anisotropic damage theory. In microscopic damage theory, an equation was proposed by Gurson[13] to promote its progress.

Some researchers have tried to solve constitutive equations with damage variables using finite element modeling (FEM), and some progress has been made in the numerical modeling of material damage.[8] Indeed, Saanouni et al.[8] introduced a single damage variable to simulate deformation localization in metal-forming processes. It is well known that the elastic properties of isotropic materials can be described by two independent elastic parameters. Therefore, it should also be possible to describe isotropic damage completely using two damage variables. It actually adds a superfluous constraint in the constitutive equations to describe the effect of damage on the two elastic parameters using a single damage variable.

In this article, the shear damage variable D_s and the bulk damage variable D_b are introduced in material constitutive equations to describe, respectively, the effect of shear damage and bulk damage on the material properties. A set of corresponding constitutive equations and numerical algorithms is proposed to form a double-variable damage model. The model is subsequently solved using a subroutine of ABAQUS.[14] Two numerical examples are given to illustrate the process of initiation and propagation, leading to deformation localization and the formation of a shear band. The numerical results are then compared with the experimental results to verify the validity of the damage model proposed in this article.

2. Elasticity and Plasticity Partially Coupled With Damage

For an isothermal process, considering full coupling between elasticity and damage as well as partial coupling be-

T.C. Lee, C.Y. Tang, and **L.C. Chan,** Department of Industrial and Systems Engineering, The Hong Kong Polytechnic University, Hung Hom, Kowloon, Hong Kong, China. Contact e-mail: mflcchan@inet.polyu.edu.hk.

tween plasticity and damage, the free-energy density function ψ can be expressed in strain space as

$$\psi = \psi_e(\varepsilon_{ij}^e, D_s, D_b) + \psi_p(p, D_s) \qquad \text{(Eq 1)}$$

where, ψ_e is the free energy associated with elastic deformation, and ψ_p is the free energy associated with hardening deformation. ψ_e can be expressed further as

$$\psi_e(\varepsilon_{ij}^e, D_s, D_b) = \psi_e^v(\varepsilon_{ij}^e, D_b) + \psi_e^d(\varepsilon_{ij}^e, D_s) \qquad \text{(Eq 2)}$$

where ψ_e^v is the free energy associated with volume elastic deformation, and ψ_e^d is the free energy associated with the shape elastic deformation. They can be expressed as

$$\rho\psi_e^v = \frac{3}{2}\sigma_m\varepsilon_m^e = \frac{9}{2}\tilde{K}(\varepsilon_m^e)^2 \frac{1}{2}(1-D_b)K(\varepsilon_{kk}^e)^2 \qquad \text{(Eq 3)}$$

$$\rho\psi_e^d = \frac{1}{2}S_{ij}e_{ij}^e = \tilde{\mu}(e_{ij}^e)^2 = (1-D_s)\mu\left[(\varepsilon_{ij}^e)^2 - \frac{1}{3}(\varepsilon_{kk}^e)^2\right] \qquad \text{(Eq 4)}$$

$$\rho\psi_p = (1-D_s)\int R(p)dp \qquad \text{(Eq 5)}$$

Here, σ_m is the hydrostatic stress, ε_m^e *is the mean elastic strain,* S_{ij} and e_{ij}^e are the deviatoric stress tensor and the elastic deviatoric strain tensor, respectively, σ_{ij} and ε_{ij}^e are the stress tensor and the elastic strain tensor, respectively, and R is the hardening function.

The laws can be obtained from the free energy Eq 1 in the following forms:

$$\sigma_{ij} = \rho\frac{\partial\psi}{\partial\varepsilon_{ij}^e} = \left[K(1-D_b) - \frac{2\mu}{3}(1-D_s)\right]Tr(\varepsilon^e)\delta_{ij} + 2\mu(1-D_s)\varepsilon_{ij}^e \qquad \text{(Eq 6)}$$

$$Y_b = \rho\frac{\partial\psi_e}{\partial D_b} = -\frac{K}{2}[Tr(\varepsilon^e)]^2 \qquad \text{(Eq 7)}$$

$$Y_s = \rho\frac{\partial\psi}{\partial D_s} = -\mu\left\{Tr[(\varepsilon^e)^2] - \frac{1}{3}[Tr(\varepsilon^e)]^2\right\} - \int R(p)dp \qquad \text{(Eq 8)}$$

In an isotropic case, the yield function can be written as

$$\tilde{\sigma}_{eq} - (\tilde{R} + \sigma_y) = 0 \qquad \text{(Eq 9)}$$

where

$$\tilde{\sigma}_{eq}\sqrt{\frac{3}{2}\tilde{S}_{ij}\tilde{S}_{ij}} = \frac{\sigma_{eq}}{1-D_s} \qquad \text{(Eq 10)}$$

$$\tilde{R} = \frac{R}{1-D_s} \qquad \text{(Eq 11)}$$

Substituting Eq 10 and 11 into Eq 9, the yield function can be rewritten as

$$\sigma_{eq} - [R + (1-D_s)\sigma_y] = 0 \qquad \text{(Eq 12)}$$

In an isotropic case and for an isothermal process, the plastic dissipation potential and the damage dissipation potential may be defined as

$$f_p = \sigma_{eq} - [R + (1-D_s)\sigma_y] \qquad \text{(Eq 13)}$$

$$\varphi_D = \varphi_{D_b} + \varphi_{D_s} \qquad \text{(Eq 14)}$$

where

$$\varphi_{D_b} = \frac{S_b}{q_b+1}\cdot\frac{1}{1-D_b}\left(-\frac{Y_b}{S_b}\right)^{q_b+1} \qquad \text{(Eq 15)}$$

$$\varphi_{D_s} = \frac{s_s}{q_s+1}\cdot\frac{1}{1-D_s}\left(-\frac{Y_s}{S_s}\right)^{q_s+1} \qquad \text{(Eq 16)}$$

From the generalized normality rule, the flow law and the evolution of the internal variables are as follows:

$$\dot{\varepsilon}_{ij}^p = \dot{\lambda}\frac{\partial f}{\partial\sigma_{ij}} = \frac{3}{2}\cdot\frac{\dot{\lambda}}{1-D_s}\cdot\frac{S_{ij}}{\sigma_{eq}} \qquad \text{(Eq 17)}$$

$$\dot{p} = \left(\frac{2}{3}\dot{\varepsilon}_{ij}^p\dot{\varepsilon}_{ij}^p\right)^{1/2} = \frac{\dot{\lambda}}{1-D_s} \qquad \text{(Eq 18)}$$

$$\dot{D}_b = -\dot{\lambda}\frac{\partial\varphi_D}{\partial Y_b} = \left(-\frac{Y_b}{S_b}\right)^{q_b}\frac{1-D_s}{1-D_b}\dot{p} \qquad \text{(Eq 19)}$$

$$\dot{D}_s = -\dot{\lambda}\frac{\partial\varphi_D}{\partial Y_s} = \left(-\frac{Y_s}{S_s}\right)^{q_s}\dot{p} \qquad \text{(Eq 20)}$$

The hardening law of metallic materials can be expressed by an exponential function:

$$R(p) = Q(1-e^{-bp}) \qquad \text{(Eq 21)}$$

And Eq 21 can be substituted into Eq 8 to yield:

$$Y_s = -\mu\left\{Tr\left[\left(\varepsilon^e\right)^2\right] - \frac{1}{3}\left[Tr\left(\varepsilon^e\right)\right]^2\right\} - Q/b\,(bp - 1 + e^{-bp}) \qquad \text{(Eq 22)}$$

Combining Eq 19, 20, 7, and 22, one can obtain

$$\dot{D}_b = \left\{\frac{\frac{K}{2}\left[Tr\left(\varepsilon^e\right)\right]^2}{S_b}\right\}\frac{1-D_s}{1-D_b}\dot{p} = \left[\frac{\sigma_m^2}{2K(1-D_b)^2S_b}\right]^{q_b}\frac{1-D_s}{1-D_b}\dot{p} \qquad \text{(Eq 23)}$$

$$\dot{D}_s = \left\{ \frac{\mu\left[Tr\left((\varepsilon^e)^2\right)\right] - \frac{1}{3}\left[Tr\left(\varepsilon^e\right)\right]^2 + \frac{Q}{b}\left(bp - 1 + e^{-bp}\right)}{S_s} \right\}^{q_s} \dot{p}$$

$$= \left[\frac{\frac{3}{2}S_{ij}S_{ij} + 6\mu\left(1 - D_s\right)^2 \frac{Q}{b}\left(bp - 1 + e^{-bp}\right)}{6\mu(1 - D_s)^2 S_s} \right]^{q_s} \dot{p} \quad \text{(Eq 24)}$$

Letting

$$f_{d1}(S_{ij}, D_s, p) = \left[\frac{\frac{3}{2}S_{ij}S_{ij} + 6\mu(1 - D_s)^2 \frac{Q}{b}(bp - 1 + e^{-bp})}{6\mu(1 - D_s)^2 S} \right]^{q_s} \quad \text{(Eq 25)}$$

$$f_{d2}(\sigma_m, D_s, D_b, p) = \left[\frac{\sigma_m^2}{2K(1 - D_b)^2 S_b} \right]^{q_b} \frac{1 - D_s}{1 - D_b} \quad \text{(Eq 26)}$$

Then,

$$\dot{D}_s = f_{d1}(S_{ij}, D_s, p)\dot{p} \quad \text{(Eq 27)}$$

$$\dot{D}_b = f_{d2}(\sigma_m, D_s, D_b, p)\dot{p} \quad \text{(Eq 28)}$$

Now, considering only the bulk damage when the hydrostatic stress is greater than $\sigma_{dth}/3$, Eq 23 can be further modified:

$$\dot{D}_b = \begin{cases} f_{d2}(\sigma_m, D_s, D_b, p)\dot{p} & \text{if } \sigma_m \geq \frac{\sigma_{dth}}{3} \\ 0 & \text{otherwise} \end{cases} \quad \text{Eq (29)}$$

In Eq 29, σ_{dth} is the stress as $\varepsilon^p = \varepsilon^p_{dth}$ and $\varepsilon^p_{dth} \geq 0$. ε^p_{dth} is the threshold value of the damage plastic strain.

3. Numerical Solution Procedures for the Damage Variables

To solve this problem, Eq 18 can be substituted into Eq 17, which gives

$$\dot{\varepsilon}^p_{ij} = 3/2 \cdot \frac{S_{ij}}{\sigma_{eq}} \dot{p} \quad \text{(Eq 30)}$$

$$S_{ij} = 2\tilde{\mu}e^e_{ij} = 2\tilde{\mu}(e_{ij} - \varepsilon^p_{ij}) \quad \text{(Eq 31)}$$

When the time $t = t_{n+1} = t_n + \Delta t$, then

$$\{\varepsilon_{ij}\}_{trial} = \{\varepsilon_{ij}\}_n + \Delta\varepsilon_{ij} \quad \text{(Eq 32)}$$

$$\{\sigma_{ij}\}_{trial} = \{\sigma_{ij}\}_n + \lambda\frac{(1 + v)(1 - D_b)_n - (1 - 2v)(1 - D_s)_n}{3v} Tr(\Delta\varepsilon)\delta_{ij} + 2\mu(1 - D_s)_n\Delta e_{ij} \quad \text{(Eq 33)}$$

$$\{S_{ij}\}_{trial} = \{S_{ij}\}_n + 2\mu(1 - D_s)_n\Delta e_{ij} \quad \text{(Eq 34)}$$

Now if,

$$\{f_p\} = \{\sigma_{eq}\}_{trial} - [R_n + (1 - D_s)_n\sigma_y] \leq 0 \quad \text{(Eq 35)}$$

Then,

$$\{\sigma_{ij}\}_{n+1} = \{\sigma_{ij}\}_{trial} \quad \text{(Eq 36)}$$

when

$$\Delta D_b = \Delta D_s = 0$$

and

$$\Delta p = 0$$

If

$$\{f_p\} = \{\sigma_{eq}\}_{trial} - [R_n + (1 - D_s)_n\sigma_y] > 0 \quad \text{(Eq 37)}$$

The stress should be "pulled" back to a new damage yield surface $\{f_p\}_{n+1}$ so that:

$$\{f_p\}_{n+1} = \{\sigma_{eq}\}_{n+1} - [R_{n+1} + (1 - D_s)_{n+1}\sigma_y] = 0 \quad \text{(Eq 38)}$$

The stress and the stress deviator on the $\{f_p\}_{n+1}$ can be given by the damage yield surface,

$$\{\sigma_{ij}\}_{n+1} = \{\sigma_{ij}\}_{trial} - 2\mu(1 - D_s)_n\Delta\varepsilon^p_{ij} \quad \text{(Eq 39)}$$

$$\{S_{ij}\}_{n+1} = \{S_{ij}\}_{trial} - 2\mu(1 - D_s)_n\Delta\varepsilon^p_{ij} \quad \text{(Eq 40)}$$

Substituting Eq 30 into Eq 39 and 40, respectively, yields the following expressions:

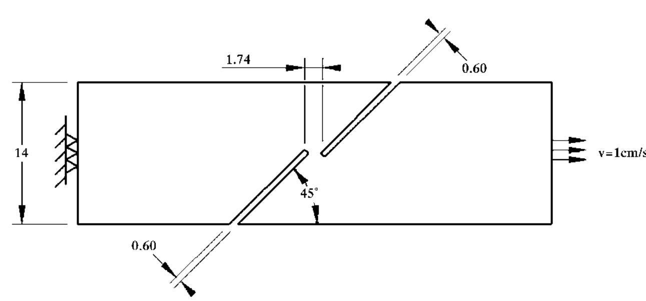

Fig. 1 Configuration of the single shear for FEM analysis (plane stress)

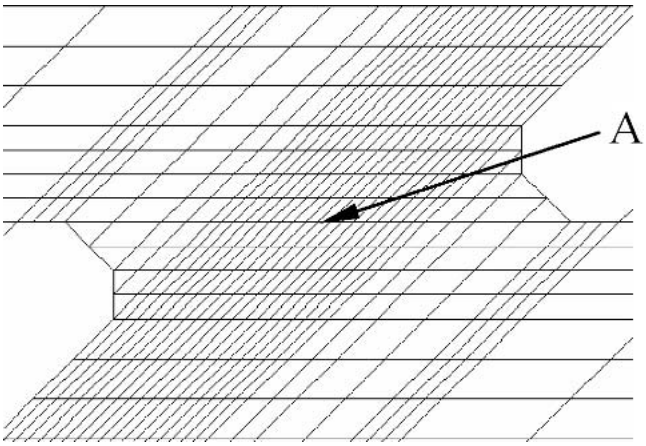

Fig. 2 Mesh around the two notches

$$\{\sigma_{ij}\}_{n+1} = \{\sigma_{ij}\}_{\text{trial}} - 3\mu(1 - D_{\text{s}})_n \cdot \frac{\{S_{ij}\}_{\text{trial}}}{\{\sigma_{\text{eq}}\}_{\text{trial}}}\Delta p \qquad \text{(Eq 41)}$$

$$\{S_{ij}\}_{n+1} = \{S_{ij}\}_{\text{trial}} - 3\mu(1 - D_{\text{s}})_n \cdot \frac{\{S_{ij}\}_{\text{trial}}}{\{\sigma_{\text{eq}}\}_{\text{trial}}}\Delta p = \{S_{ij}\}_{\text{trial}}\left[1 - 3\mu(1 - D_{\text{s}})_n \cdot \frac{\Delta p}{\{\sigma_{\text{eq}}\}_{\text{trial}}}\right] \qquad \text{(Eq 42)}$$

Taking the inner product of Eq 42 and considering Eq 38,

$$\{R\}_{n+1} + (1 + D_{\text{s}})_{n+1}\sigma_y = \{\sigma_{\text{eq}}\}_{\text{trial}}\left[1 - 3\mu(1 - D_{\text{s}})_n \cdot \frac{\Delta p}{\{\sigma_{\text{eq}}\}_{\text{trial}}}\right] \qquad \text{(Eq 43)}$$

The nonlinear Eq 43 can be resolved by Newton's method. The steps are as follows:

(1) $\Delta p_0 = 0$

(2) $\{\Delta D_{\text{s}}\}_0 = 0$

(3) $\{\Delta D_{\text{b}}\}_0 = 0$

(4) $\sigma_{\text{eq}} = \{\sigma_{\text{eq}}\}_{\text{trial}}$

(5) if $\{\sigma_{\text{eq}}\} - [R + (1 - D_{\text{s}})\sigma_{\text{y}}] \leq r\sigma_{\text{y}}$ then stop iteration, otherwise turn to step (6) (Eq 44)

(6) $c_k = \dfrac{\{\sigma_{\text{eq}}\} - [R + (1 - D_{\text{s}})\sigma_{\text{y}}]}{h + 3\mu(1 - D_{\text{s}}) - \sigma_{\text{y}} f_{\text{d1}}}$

(7) $\Delta p_{k+1} = \Delta p_k + c_k$

(8) $\{\Delta D_{\text{s}})_{k+1} = \{\Delta D_{\text{s}}\}_k + f_{\text{d1}} \cdot c_k$

(9) $\{\Delta D_{\text{b}}\}_{k+1} = \{\Delta D_{\text{b}}\}_k + f_{\text{d2}} \cdot c_k$

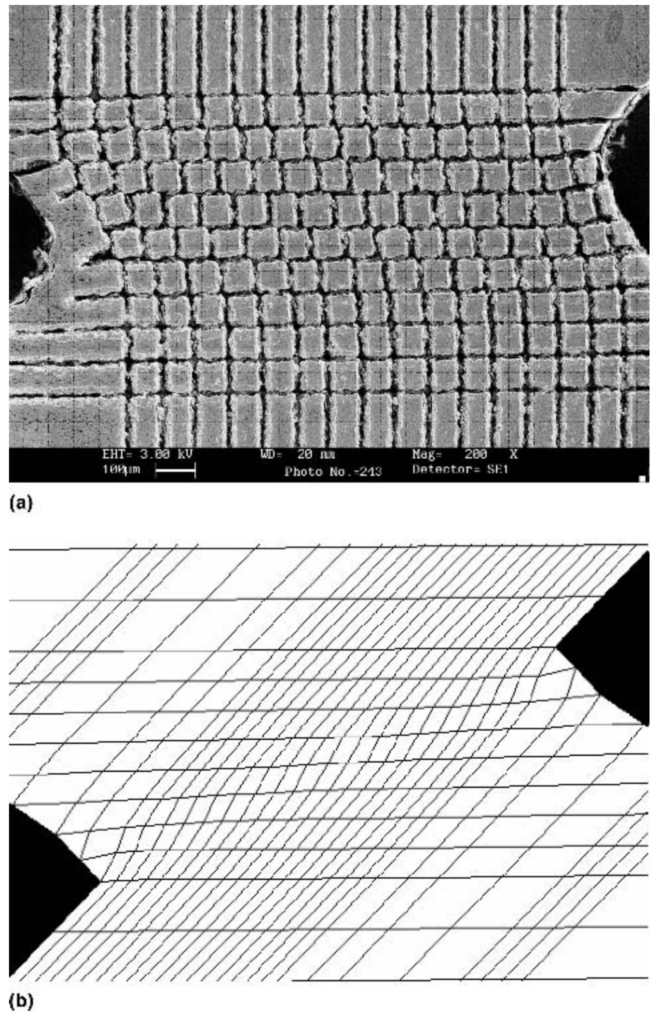

Fig. 3 Deformation distribution at $d = 0.386$ mm: **(a)** SEM graph; and **(b)** computational result

(10) $S_{ij} = \{S_{ij}\}_{\text{trial}} - 3\mu(1 - D_{\text{s}})_n \cdot \Delta p_{k+1}$

(11) $\sigma_{\text{eq}} = \sqrt{\frac{3}{2} S_{ij} S_{ij}}$

(12) Turn to step (5)

where

$$h = \frac{dR}{dp} \qquad (45)$$

Thus, the new stress and damage state on the new damage yield surface $\{f_{\text{p}}\}_{n+1}$ has been obtained.

4. Numerical Modeling of the Shear Damage in the Shear Deformation Localization Region

In this article, aluminum 2024T3 was considered in the numerical modeling of the shear damage. The modeling of the

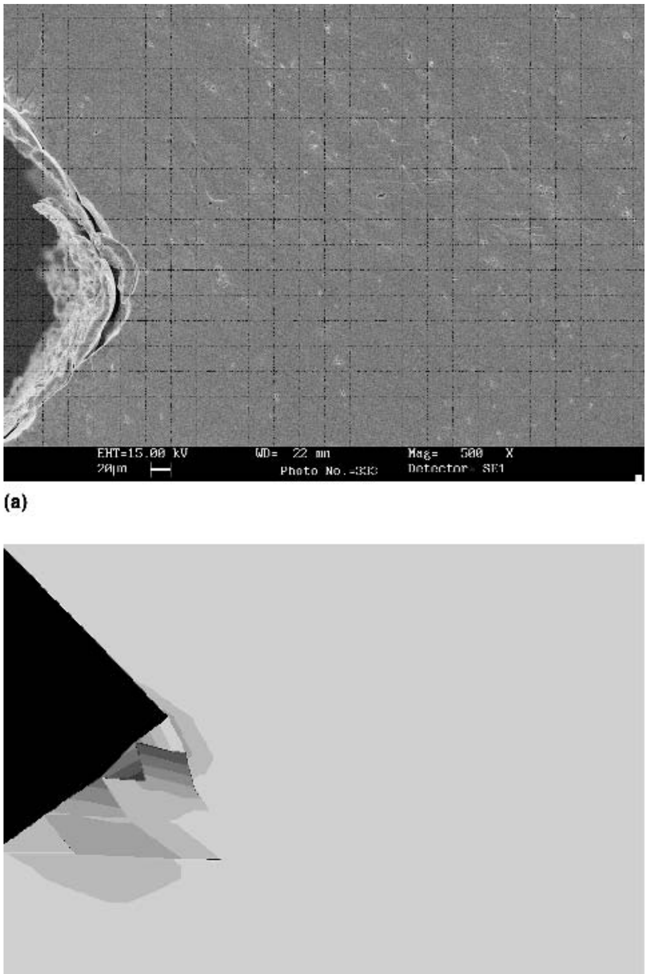

(a)

(b)

Fig. 4 Bulk damage state at the tip of notch (d = 0.394 mm): **(a)** SEM graph; and **(b)** computational result

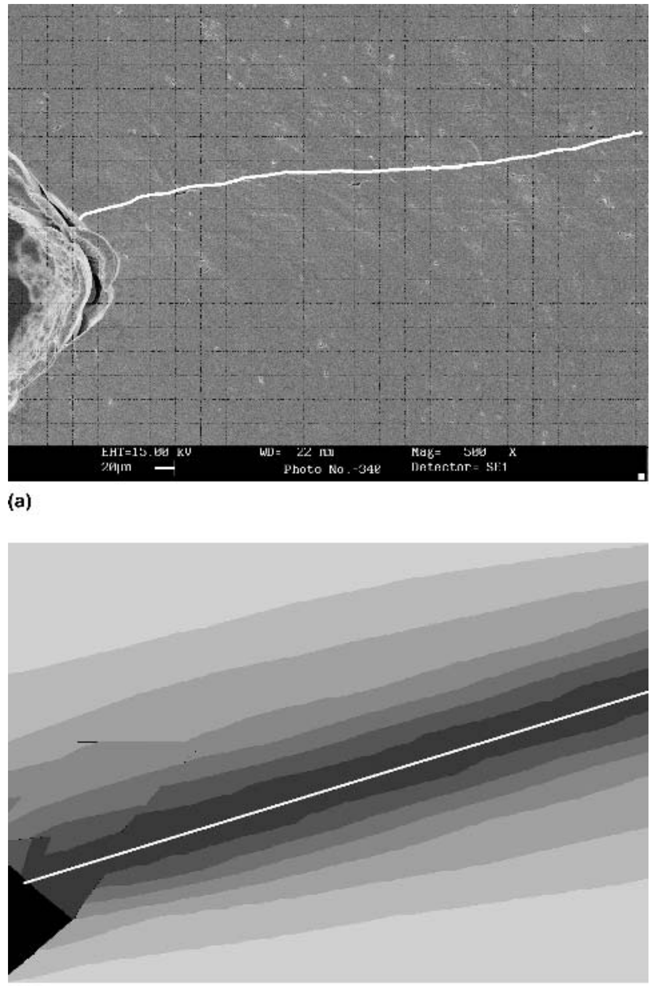

(a)

(b)

Fig. 5 Failure path: **(a)** SEM graph; and **(b)** computational result

Table 1 The mechanical properties of aluminum 2024T3

Young's modulus (E), MPa	v	σ_y, MPa	ε^p_{dth}, %	D_{bcr}
74,760	0.34	372.19	1.88	0.667
S_b, MPa	**q_b**	**D_{scr}**	**S_s, MPa**	**q_s**
0.762977	−1.149988	0.205	2.8714214	−0.3655015
Q, MPa	**b**			
201.318	15.395			

(E), Young's modulus; v, Poisson ratio; σ_y, yield stress; ε^p_{dth}, threshold value of the damage plastic strain; D_{bcr}, critical bulk damage variable; D_{scr}, critical shear damage variable; b, hardening index; s_b, q_s, and Q, material constants

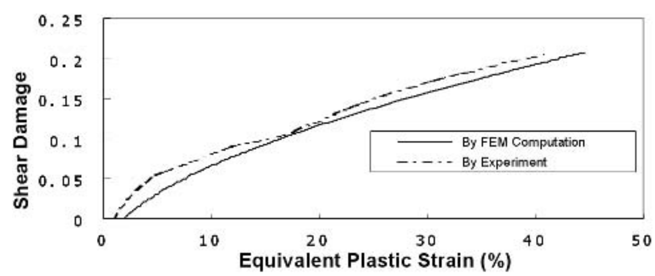

Fig. 6 Damage-equivalent plastic strain curve

shear damage was made for the single shear test and the side pressing. In the two computational examples, the shear damage is the main damage. The numerical computation in this article was completed by ABAQUS/Explicit.[14] The modeling framework developed in this article was applied in the user subroutine VUMAT. Through a series of tests, the mechanical properties were obtained as shown in Table 1. In the following two computational examples, aluminum 2024T3 was considered.

4.1 Numerical Modeling of the Single Shear

The single shear test is a standard for testing the shear properties of an aluminum alloy according to the ASTM standard B 831-93.[15] The geometry and loading conditions of the single shear test are shown in the Fig. 1. The zone between the

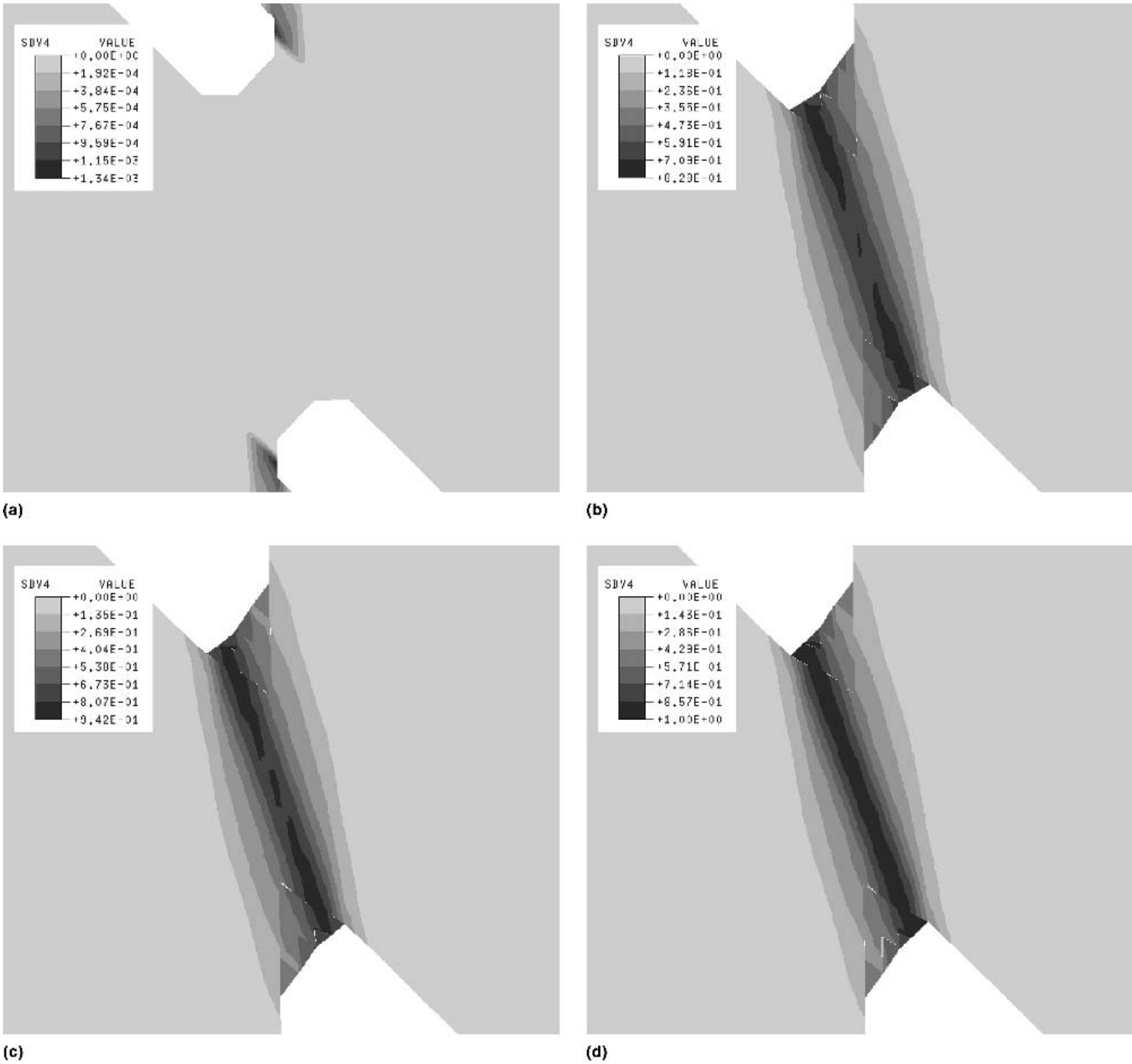

Fig. 7 Evolution of the shear damage field: **(a)** $d = 0.104$ mm; **(b)** $d = 0.353$ mm; **(c)** $d = 0.374$ mm; and **(d)** $d = 0.394$ mm

two notches was divided into very fine elements. The finite element mesh around the notches is given in Fig. 2. The scanning electron microscope (SEM) micrographs in Fig. 3-5 were obtained by in situ SEM single shear tests.

The experimental and computational results of the deformation distribution between the two notches are shown, respectively, in Fig. 3(a) and (b), corresponding to the displacement $d = 0.386$ mm. The comparability of the deformation distribution between the two notches for the experimental and computational results can be seen in Fig. 3(a) and (b).

In Fig. 4(a), the damage state at the tip of a notch in an in situ SEM test is shown. In Fig. 4(a), it can be seen that the failure at the tip of a notch is caused by bulk damage. In Fig. 4(b), the bulk damage distribution at the tip of the notch obtained from numerical computation is shown. Comparing Fig. 4(a) and (b), the computational result is coincident with the experimental result.

In Fig. 5(a), the failure path is marked by examining the fracture section. The path of the shear damage failure by numerical computation is shown in Fig. 5(b). Comparing Fig. 5(a) and (b), it can be seen that the computational result is coincident with the experimental result for the failure path.

In Fig. 6, two damage equivalent plastic strain curves are shown. One of them was obtained through the single shear test, while the other was obtained by numerical computation of shear damage for the mesh near point A, which is shown in Fig. 2. As a result, the computational curve seems to be quite consistent with the test result.

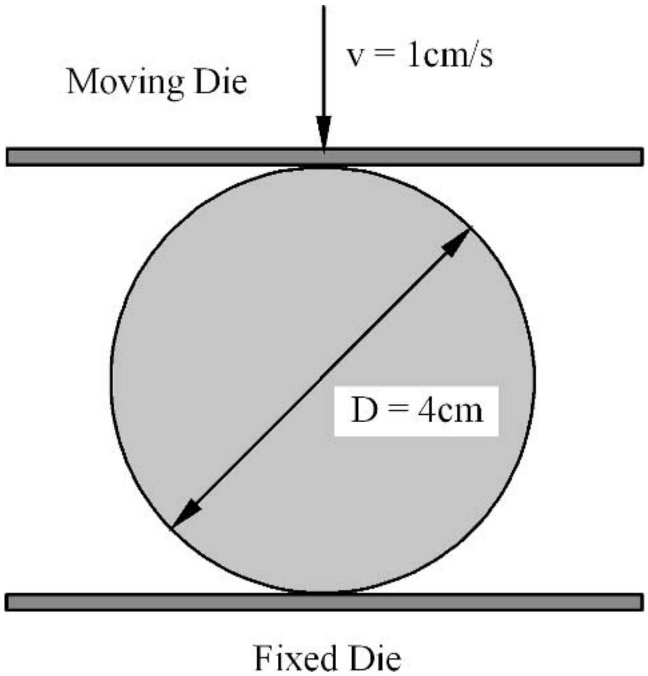

Fig. 8 Configuration of the side pressing for FEM analysis (plane strain)

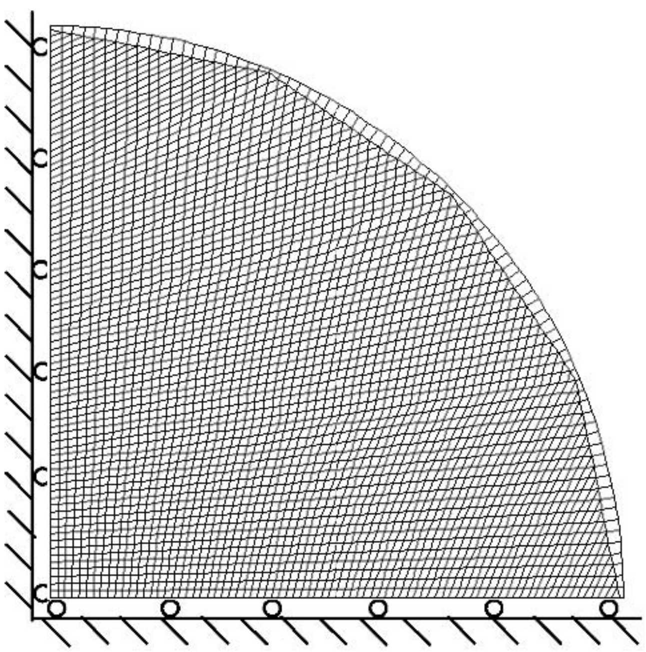

Fig. 9 Mesh and the boundary condition of the side pressing

In Fig. 7, the evolution of the shear damage field is shown. The initiation of the shear damage and the evolution of the shear damage in the shear deformation localization process are shown in Fig. 7(a)-(d). During the first stage, the maximum shear damage was concentrated around the notches, as shown in Fig. 7(a). With the increase of displacement d, the maximum shear damage shifted to the middle position between the two notches, which is shown in Fig. 7(b). The three areas of maximum shear damage coalesced to form a shear band that led to failure, as shown in Fig. 7(c) and (d). In Fig. 7, $SDV4 = D_s/D_{scr}$. In the areas with considerable shear damage, material softening and shear deformation localization occurred. With the increase of the shear damage, the shear deformation localization became more serious, and the shear band was formed.

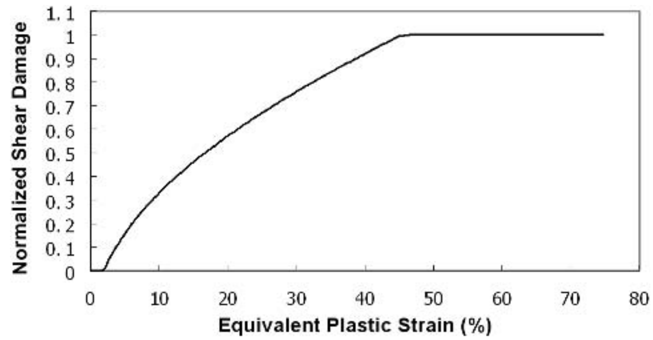

Fig. 10 Evolution curve of the shear damage-equivalent plastic strain

4.2 Numerical Modeling of the Side Pressing of a Cylinder (Plane Strain)

Side pressing is a machining process that is often used in industry. A plane strain cylinder is side pressed by a moving die into a fixed one, as shown in Fig. 8. The geometry and loading conditions of the side-pressing cylinder are also shown in the figure. The finite element mesh and the boundary condition in the computational example are shown in Fig. 9.

In the computational example, the bulk damage is constant and is equal to zero. The evolution curve of shear damage-equivalent plastic strain at the cylinder center is given in Fig. 10. The evolution of the shear damage field of the cylinder is shown in Fig. 11.

In Fig. 11, the positions indicated by arrows are the positions where maximum shear damage occurs. It was found that the position of maximum shear damage changed with the displacement of the moving die. When displacement d was smaller than 6.0 mm, the maximum shear damage appears on or near the top of the cylinder, as shown in Fig. 11(a)-(d). With an increase in displacement d, the maximum shear damage shifts to the center of the cylinder, as shown Fig. 11(e) and (f). When $d = 5.0$ mm, the first shear band appears, as shown in Fig. 11(c), and when $d = 5.5$ mm, the second shear band appears, as shown in Fig. 11(d). With further increases in displacement d, the second shear band propagates, leading to failure, as shown in Fig. 11(e) and (f). In Fig. 11, $SDV4 = D_s/D_{scr}$.

5. Discussion

In this study, a double-variable damage model was applied. In the model, two damage variables, D_b and D_s, were introduced into the constitutive equations. The two damage variables were independent of each other. They had the corresponding physical significance. Compared with the

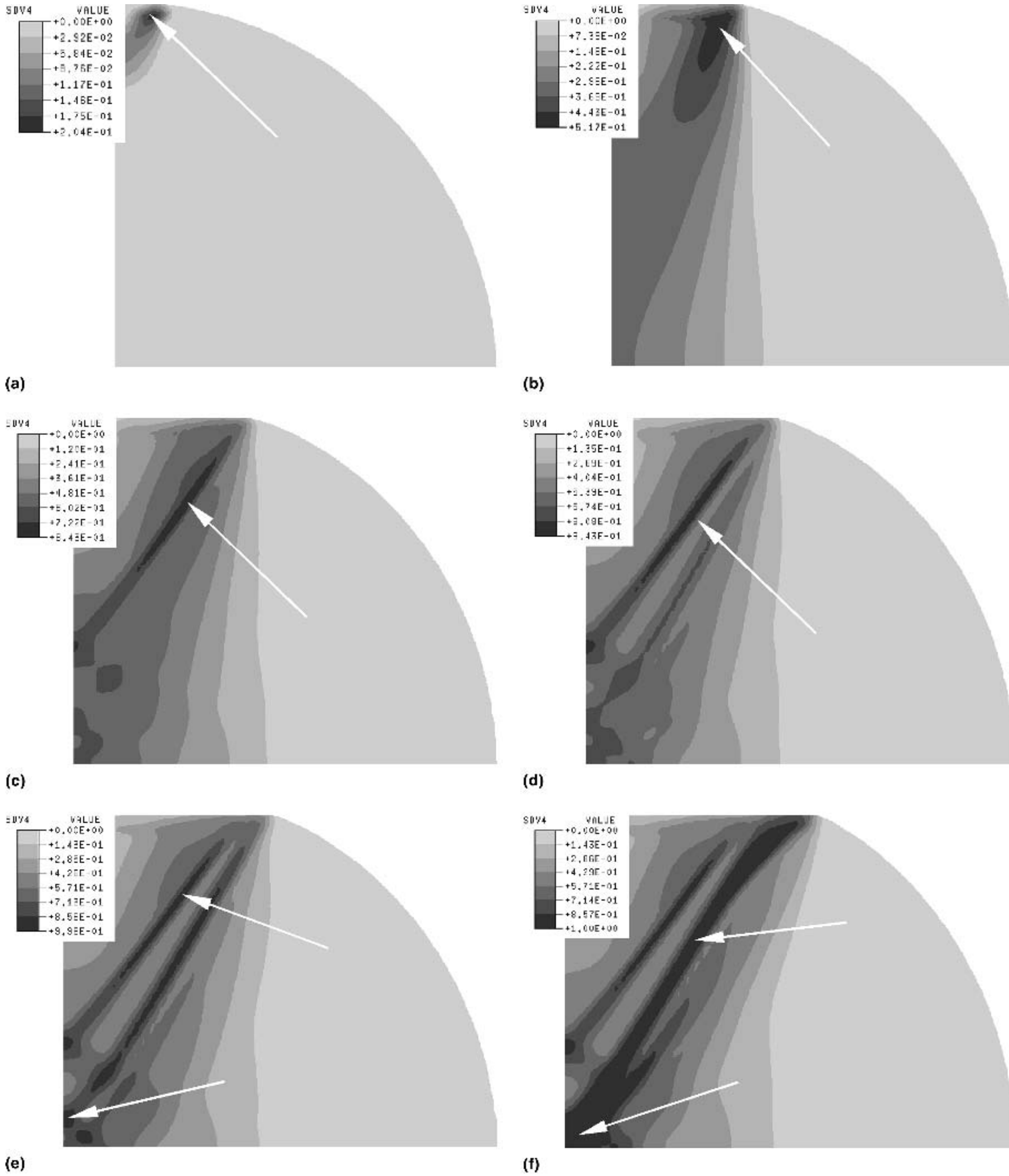

Fig. 11 Evolution of the shear damage in the side-pressing process: **(a)** $d = 0.5$ mm; **(b)** $d = 3.0$ mm; **(c)** $d = 5.0$ mm; **(d)** $d = 5.5$ mm **(e)** $d = 6.0$ mm; and **(f)** $d = 7.5$ mm

single-variable damage model, this model degenerates to the single-variable damage model if $D_b = D_s$. Therefore, the double-variable damage model is suitable for studying the damage caused by shear, especially damage in the shear bands, because there is no superfluous constraint $D_b = D_s$.

After introducing a shear damage variable D_s, the effect of the shear damage on shear stiffness can be demonstrated by the constitutive equations. The relative softening of material induced by the damage to material can be considered. Therefore, the whole process of formation and propagation of shear bands to failure can be preferably modeled after introducing a shear damage variable, D_s.

In Eq 12, it was observed that the yield function relates only to the shear damage variable D_s. Equation 12 is derived from the von Mises yield function. The von Mises yield function is a shear-type yield function. Therefore, it is reasonable that the yield function in this article relates to the shear damage variable D_s.

The side-pressing example is the typical computational example for shear banding. In Saanouni et al.,[8] the example was computed by FEM using the single-variable damage model. The example in this article cannot be compared directly with that example because different materials were used. However, it is possible that more than one shear band may occur in the side-pressing process.

6. Conclusions

As revealed by the experimental and computational results, the damage variables D_s and D_b are suitable to be used to describe, respectively, the shear damage and the bulk damage in the isotropic elasto-plastic damage state. The numerical computational results obtained by applying the damage model, as proposed in this article, are coincident with the experimental results. It is demonstrated that the model in this article is applicable.

To introduce the shear damage variable D_s into the constitutive equations can model the relative softening of the material and the shear deformation localization induced by shear damage. By using the numerical model in this article, it is possible to simulate the whole process of the formation and propagation of shear bands to failure that may occur in metal forming.

Acknowledgment

The work described in this article was substantially supported by a grant from the Research Grants Council of the Hong Kong Special Administrative Region (Project No. PolyU 5131/98E).

References

1. C.Y. Tang, T.C. Lee, B. Roa, and C.L. Chow, An Experimental Study of Shear Damage Using In-Situ Shear Test, *Int. J. Damage Mech.,* Vol 11, 2002, p 335-353
2. Z.H. Chen, L.C. Chan, T.C. Lee, and C.Y. Tang, An Investigation on the Formation and Propagation of Shear Band in Fine-Blanking Process, *J. Mater. Proc. Technol.,* Vol 138, 2003, p 610-614
3. R. Hill, Acceleration Waves in Solids, *J. Mech. Phys. Solids,* Vol 10, 1962, p 1-16
4. J.R. Rice, The Localization of Plastic Deformation, *Proceedings of 14th International Congress Theoretical and Applied Mechanics*, W.T. Koiter, Ed., (Amsterdam, New York), North-Holland, 1977
5. M. Bruknig, S. Berger, and H. Obrecht, Numerical Simulation of the Localization Behavior of Hydrostatic-Stress-Sensitive Metals, *Int. J. Mech. Sci.,* Vol 42, 2000, p 2147-2166
6. C.Y. Tang, C.L. Chow, W. Shen, and W.H. Tai, Development of a Damage-Based Criterion for Ductile Fracture Prediction in Sheet Metal Forming, *J. Mater. Proc. Technol.,* Vol 91, 1999, p 270-277
7. C.Y. Tang and W.H. Tai, Material Damage and Forming Limits of Textured Sheet Metals, *J. Mater. Proc. Technol.,* Vol 99, 2000, p 135-140
8. K. Saanouni, K. Nesnas, and Y. Hammi, Damage Modeling in Metal Forming Processes, *Int. J. Damage Mech.,* Vol 9, 2000, p 196-240
9. J. Lemaitre, Coupled Elasto-Plasticity and Damage Constructive Equations, *Comput. Methods Appl. Mech. Eng.,* Vol 51, 1985, p 31-49
10. C.L. Chow and J. Wang, An Anisotropic Theory of Elasticity for Continuum Damage Mechanics, *Int. J. Fract.,* Vol 33, 1987, p 3-16
11. C.L. Chow and J. Wang, An Anisotropic Theory of Continuum Damage Mechanics for Ductile Fracture, *Eng. Fract. Mech.,* Vol 27, 1987, p 547-558
12. C.L. Chow and J. Wang, Ductile Fracture Characterization With an Anisotropic Continuum Damage Theory, *Eng. Fract. Mech.,* Vol 30, 1988, p 547-563
13. A.L. Gurson, Continuum Theory of Ductile Rupture by the Void Nucleation and Growth, *J. Eng. Mater. Technol.,* Vol 99, 1977, p 2-15
14. Anon., *ABAQUS/Explicit User's Manual (Version 5.8),* Hibbitt, Karlsson & Sorensen, Inc, 1998
15. "Standard Test Method for Shear Testing of Thin Aluminum Alloy Products," B 831-93, *1996 Annual Book of ASTM Standards,* Vol 02.02, *Aluminum and Magnesium Alloys,* ASTM, p 590-592